Timelapse ultrasonic tomography for measuring damage localization in geomechanics laboratory tests.

Tudisco, Erika; Roux, Philippe; Hall, Stephen; Viggiani, Giulia M.B; Viggiani, Gioacchino

Published in:
Journal of the Acoustical Society of America

DOI:
10.1121/1.4913525

2015

Timelapse ultrasonic tomography for measuring damage localization in geomechanics laboratory tests

Erika Tudisco[a)]
University Grenoble Alpes, 3SR, F-38000, Grenoble, France

Philippe Roux
Institut des Sciences de la Terre, Université Joseph Fourier and Centre National de la Recherche Scientifique, Grenoble, France

Stephen A. Hall
Division of Solid Mechanics, Lund University, Lund, Sweden

Giulia M. B. Viggiani
Dipartimento di Ingegneria Civile e Ingegneria Informatica, Università di Roma Tor Vergata, Roma, Italy

Gioacchino Viggiani
University Grenoble Alpes, 3SR, F-38000, Grenoble, France

(Received 19 June 2014; revised 9 January 2015; accepted 28 January 2015)

Variation of mechanical properties in materials can be detected non-destructively using ultrasonic measurements. In particular, changes in elastic wave velocity can occur due to damage, i.e., micro-cracking and particles debonding. Here the challenge of characterizing damage in geomaterials, i.e., rocks and soils, is addressed. Geomaterials are naturally heterogeneous media in which the deformation can localize, so that few measurements of acoustic velocity across the sample are not sufficient to capture the heterogeneities. Therefore, an ultrasonic tomography procedure has been implemented to map the spatial and temporal variations in propagation velocity, which provides information on the damage process. Moreover, double beamforming has been successfully applied to identify and isolate multiple arrivals that are caused by strong heterogeneities (natural or induced by the deformation process). The applicability of the developed experimental technique to laboratory geomechanics testing is illustrated using data acquired on a sample of natural rock before and after being deformed under triaxial compression. The approach is then validated and extended to time-lapse monitoring using data acquired during plane strain compression of a sample including a well defined layer with different mechanical properties than the matrix.
 [http://dx.doi.org/10.1121/1.4913525]

[KGS] Pages: 1389–1400

I. INTRODUCTION

This work focuses on the application of ultrasonic tomography to the experimental characterization of localized deformation (shear bands, compaction bands, and fractures) in sedimentary rocks such as sandstones. Sandstones are cemented granular materials that commonly form subsurface reservoirs for hydrocarbons. Understanding the deformation processes in these rocks is important for the success and safety of reservoir engineering operations including hydrocarbons extraction and geological sequestration of CO_2. As with other cemented granular materials, the deformation and failure of sandstones involves a number of processes including porosity reduction and damage (micro-cracking, cement degradation, and grain breakage). Porosity reduction can lead to increases of stiffness and thus increased elastic wave propagation velocity while damage has the opposite effect. These deformation and degradation processes do not occur homogeneously and generally focus into localized deformation zones. Furthermore, sandstones are naturally heterogeneous materials. Thus, the characterization of the mechanical properties and the mechanisms of deformation in these materials are challenging and require experimental techniques that can provide details on the different mechanisms and the associated spatio-temporal evolution of the mechanical properties. In this context, this paper presents new approaches to use ultrasonic velocity measurements to characterize heterogeneous distributions, and evolution thereof, of the mechanical properties of cemented granular materials such as sandstone.

Strain and damage localization in rocks such as sandstones have been traditionally investigated using microscopy analysis of "thin sections" cut from deformed specimens. This approach is clearly destructive, and thus cannot be employed to study evolving processes and, in addition, can only provide indirect analysis of deformation and damage through geometrical measurements, e.g., of crack density. In recent years, the use of non-destructive and non-invasive techniques has been developed in experimental geomechanics.[1,2] These techniques include x-ray tomography and Digital Image Correlation (DIC) of two-dimensional (2D) or three-dimensional (3D) (volume) images. Both of these have

[a)]Author to whom correspondence should be addressed. Present address: Division of Solid Mechanics, Lund University, Lund, Sweden. Electronic mail: erika.tudisco@solid.lth.se

proven to be powerful tools in the study of heterogeneous phenomena, in particular, DIC provides direct quantification of strain fields throughout test specimens, but does not, however, provide data on changes of mechanical properties. Acoustic and ultrasonic measurements have also been long used in experimental geomechanics, for example, to characterize anisotropy and the evolution of elastic wave velocities during rock deformation experiments. However, such methods have generally been limited in their spatial sampling of the study materials and heterogeneity is, in general, neglected. At the geological scale, seismic imaging has been a standard practice in both academic and industrial investigations of the Earth's sub-surface for many years. Of the seismic imaging techniques used in such investigations, seismic tomography has significant interest for mechanics, as it provides mapping of velocity heterogeneity in a study region (e.g., Iyer and Hirahara[3]). Such maps of seismic velocity can provide insight into variations in mechanical properties due to both rock property variations and deformation. In this work the concepts of seismic tomography are applied at a much smaller scale, i.e., that of geomechanical laboratory experiments (centimeter scale), using ultrasonic measurements to map deformation-induced velocity heterogeneity, and its evolution with loading, in rock samples.

Seismic tomography involves inverse analysis procedures to determine wave propagation velocities from travel-times (or attenuation properties from amplitudes). Many approaches to solve the inversion problem have been proposed for different geometries; these include using ray-theoretical assumptions, with curved ray tracing to account for heterogeneous velocity structure (e.g., Berryman[4]), the use of "wavepaths" (e.g., Vasco and Majer,[5] Van Schaack[6]) and, more recently, full-waveform inversion approaches (e.g., Brossier *et al.*,[7] Virieux and Operto[8]). Extensions have also been made, for example, to include anisotropy (e.g., Chapman and Pratt[9,10]), which could be intrinsic or deformation induced. Here, in addition to an adaptation of seismic tomography techniques for application at the laboratory scale, new approaches to the data handling and inverse analysis are presented, which are of relevance to both laboratory and larger-scale applications.

The basis of the approach presented in this paper is cross-hole seismic tomography adapted to laboratory tests using ultrasonic frequency waves to characterize spatio-temporal variations in ultrasonic propagation velocities inside study specimens. The ultimate aim is to employ this technique to understand better the mechanisms of deformation and damage that control the mechanical behavior of the material, as discussed by Hall.[11] Previous publications on laboratory scale ultrasonic tomography have generally not yielded satisfactory resolution to provide a robust tool for such experimental characterization. For example, Debski and Young[12] used 24 emitter/receiver transducers to image a horizontal section of a cylindrical granite sample (diameter 300 mm and height of 200 mm) that had been previously heated to induce damage. A low velocity (damaged) area surrounding a main crack could be visualized, but good resolution was only possible by using a combined velocity-attenuation tomography, which implied losing the physical connection of the measurement to the rock-properties. Scott and Abousleiman[13] used two arrays of ten transducers to register acoustic signals propagating across a vertical plane of a cylindrical sample of porous limestone during triaxial compression (sample dimensions were: Diameter 152 mm and height 267 mm). An increase of propagation velocity was observed during the isotropic compression and, during deviatoric loading, a diffuse low velocity zone developed that localized to form an inclined band as the sample started to yield. Lee *et al.*[14] developed a system to transmit and acquire shear waves using a set of bender elements placed on a rigid frame, with about ten transducers per side. The system was installed within a true triaxial apparatus and allowed the detection of velocity anomalies inside the sand sample. The dimensions of the sample were 365×270 mm^2, which are relatively large compared to the size of conventional samples in rock/geo-mechanics. Mitra and Westman[15] conducted an experimental study combining numerical modeling and 3D ultrasonic tomography on a cylindrical sample of Berea sandstone with a diameter of 50.8 mm and a height of 101.6 mm tested under uniaxial compression. Fifteen source transducers and 18 receiver transducers were placed around the sample to obtain a 3D image of the velocity field. However, it was not possible to identify the failure plane in the resultant tomography. Using an acquisition setup similar to the first example in this paper, Charalampidou *et al.*[16,17] investigated the formation and evolution of shear and compaction bands in cylindrical samples of Vosges sandstone (diameter of 38–50 mm and height of 76–100 mm) under triaxial compression. Ultrasonic tomography was used in conjunction with other full-field methods and the comparison between the different techniques showed that ultrasonic tomography is able to locate the damaged regions in a sample and that the propagation velocity decreases with increasing macroscopic strain. However, resolution of the ultrasonic tomography was limited and potential artifacts from the inversion produced uncertainties in the interpretation.

Key challenges, highlighted in the examples presented above, are achieving sufficient spatial and temporal resolution of the velocity field, even in the presence of significant heterogeneity, and minimizing reconstruction artifacts to enable characterization of the phenomena of interest. In this work, new procedures to identify arrival times and to perform their inversion to map the velocity field inside test samples are presented. These procedures are illustrated using results obtained on a sample of natural rock (sandstone from the Vosges mountains in France[18]) before and after deformation by triaxial compression. Validation of the methodology is provided using data acquired for a controlled-geometry sample of rock (Fontainebleau sandstone) that contains an artificially-created and well-defined layer with different mechanical properties. The approach is subsequently extended to provide time-lapse imaging of the velocity field evolution during deformation of the controlled-geometry sample under plane strain compression.

II. EXPERIMENTAL SETUP AND DATA ACQUISITION SYSTEM

The ultrasonic data acquisition involved two arrays of ultrasonic transducers placed facing each other and in

contact with two opposite faces of a sample, as shown schematically in Fig. 1. Two types of arrays were used, consisting of either 32 or 64 piezoceramic transducers, which both provided a large amount of data and thus the potential for well-resolved imaging. These transducers, originally designed to work in water, can generate and detect displacements perpendicular to their contacting faces. Such displacements can clearly be generated by compressional (P-) waves, but also by inclined S-waves. In this work only the first arrival for each source-receiver pair has been taken into account, and this can be confidently associated to a P-wave. A molasses (Couplant SCW by SOFRANEL) was used to ensure the coupling between the arrays and the tested sample. The dimensions of the transducers were 15 and 20 mm wide and 1.5 and 0.75 mm high, respectively [see Fig. 1(c)]. This makes the transducers to be omnidirectional in the plane defined by the source-receiver arrays and very collimated in the perpendicular direction. The choice between the two types of arrays depended on the material being studied and the frequency of the signals that could propagate. While it is desirable to use a relatively high frequency to increase spatial resolution, practically the frequency that can be used is limited by grain dimensions and material stiffness. In this case the optimum central frequency was found to be 1 MHz for the natural sandstone sample and measurements were made using the 64-transducer arrays, while, for the controlled-geometry sample the 32-transducer arrays (central frequency of 0.5 MHz), were used. The signals were generated and received using a 64 channel emitter-receiver LeCoeur system. The signal emitted by every source was a broadband pulse at the central frequency of the transducer.

During the experiments one array of transducers worked as the sources and the other as the receivers. More specifically, signals were emitted from each element in the source array, in turn, and recorded, independently, at all of the elements in the receiver array. Signals were acquired with a sampling frequency of 20 MHz for around 45 μs. To increase the signal-to-noise ratio and get statistically relevant data the signals were averaged over 200 acquisitions. This procedure has been carried out *pre* and *post-mortem*, i.e., before and after a sample has been mechanically tested, or during loading, which is commonly referred to as "*in situ*." In the latter case each data set, consisting of 32×32 signals, required an acquisition time of 7 s plus 45 s of readout.

The described data acquisition generates a huge amount of data (64×64 or 32×32), which, when the acquisition is carried out *pre*/*post-mortem* can be further multiplied by shifting the arrays to cover the entire height of larger specimens [Figs. 1(a) and 1(b)]. However, signals corresponding to two transducers far from one another typically had a low amplitude and hence a low signal-to-noise ratio, making it difficult to extract travel-times from these recordings. Despite this, the usable data still provide a very good spatial coverage of the sample, as indicated later.

The data analysis procedures are described in Sec. III using data obtained from a sample of Vosges sandstone before and after triaxial compression at a confining pressure of 30 MPa (see Tudisco[19] for details). The test specimen was an 80 mm long cylinder with diameter of 38 mm, which had been cut to obtain 2 parallel flat vertical surfaces 20 mm wide against which the transducer arrays could be placed, as shown in Fig. 1(d). To encourage strain localization in the central part of the specimen, 2 notches of about 2 mm depth were cut in the flat surfaces. The deformation experiment was interrupted immediately after the peak deviatoric stress (at an overall axial strain of 1%), which indicated macroscopic failure of the sample.

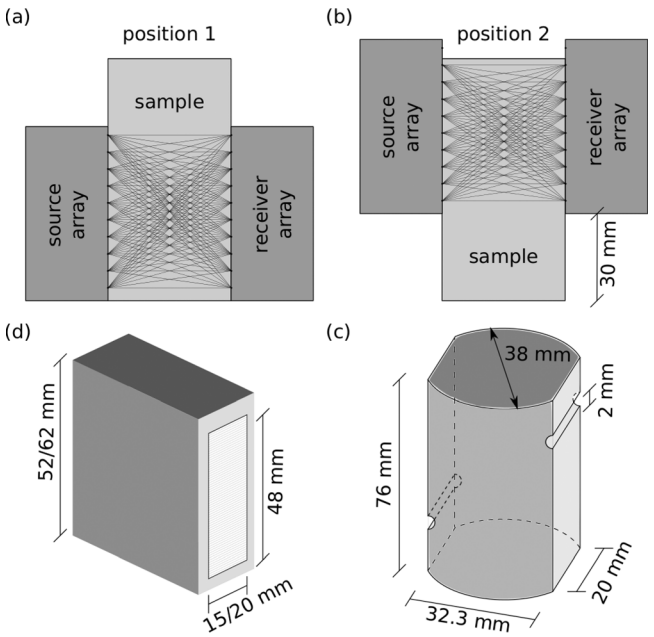

FIG. 1. Schematic of the ultrasonic data acquisition (a) and (b); to cover the entire height of the specimen two positions for the arrays are used. Schematic of an array of transducers (c) and of the natural rock sample (d).

III. DATA ANALYSIS

An example of the acquired signals, transmitted through the sample of natural rock, is presented in Fig. 2. The figure shows the signals generated by the central transducer of the source array and registered at the 64 transducers of the receiving array in position 1, i.e., when the two arrays are positioned at the bottom of the sample [see Fig. 1(c)]. Figures 2(a) and 2(b) are from the intact and deformed state, respectively, i.e., *pre*/*post-mortem*. These images show that the strain localization in the sample strongly affects wave propagation producing increased travel times or reduced velocities, distorted wave fronts, and multiple propagation paths, leading to at least two wave fronts. Signals received at transducers 25 to 35 result from the destructive interference of the two wave fronts so that, with standard approaches, no useful travel time data can be extracted. The loss of information is particularly problematic as these signals correspond to ray-paths crossing the more intensely deformed portion of the sample, which is the region of interest. To overcome this issue, a double beam forming (DBF) approach has been implemented that allows manipulation of the data to identify and isolate the different arrivals and, therefore, enables picking of arrival times of waves traversing the area of interest,

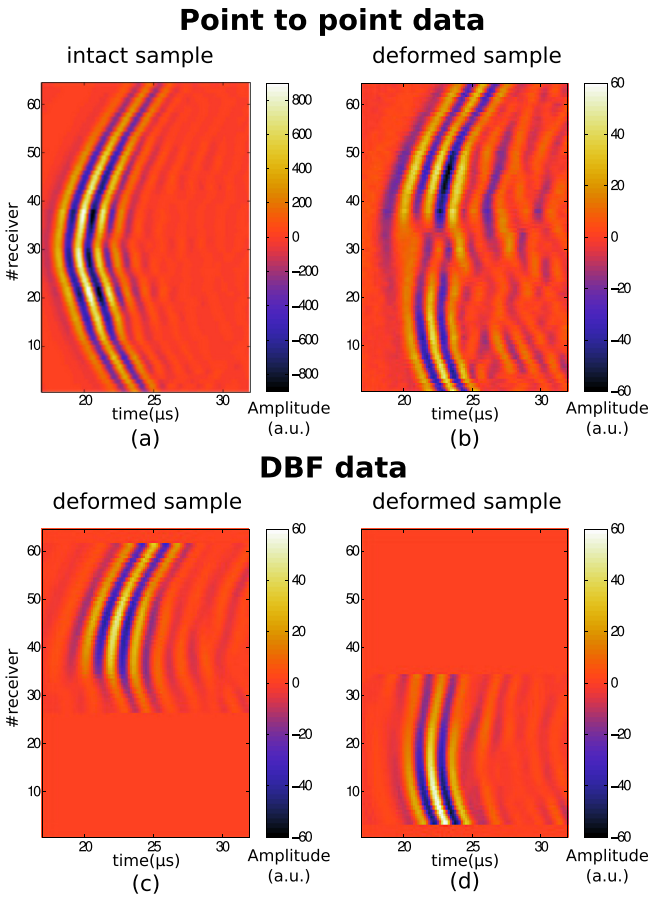

FIG. 2. (Color online) Example of experimental data obtained from propagation through an intact (a) and a deformed sample (b), corresponding to a source located at position 32 (the center of the array) and all receivers. In the case of a deformed sample, the data show two wave fronts that interfere destructively. DBF data [(c) and (d)] obtained using subarrays of five transducers; the two sets of data correspond to two different spots in the 3D DBF matrix at different θ_r, θ_s positions (see Fig. 4). The two wave fronts can be isolated completely.

including multiple arrivals for individual source-receiver subarray pairs. The DBF approach is described in Sec. III A.

A. DBF

Beamforming is an array processing technique used for the detection and separation of signals and improvement of signal-to-noise ratio. In this work time-delay beamforming is applied simultaneously at the source and receiver arrays thus double beamforming, in a similar way to described by Roux *et al.*[20]

The DBF processing can be formulated in the time domain as

$$p_{\mathrm{DBF}}(t,\,\theta_r,\,\theta_s) = \frac{1}{N_r N_s}\sum_{i=1}^{N_r}\sum_{j=1}^{N_s} p\big(t + \tau(\theta_r,\,y_{ri}) + \tau\big(\theta_s,\,y_{sj}\big),\,y_{ri},\,y_{sj}\big), \tag{1}$$

where $p(t,\,y_{ri},\,y_{sj})$ is the pressure measured by the transducer at time t, at a receiving position y_{ri}, and source position y_{sj}, N_r/ N_s are the number of transducers in the receiver/source subarray and θ_r/θ_s are the arrival/take-off angles. The time delay, $\tau(\theta,\,y)$, is defined as

$$\tau(\theta,\,y) = \frac{(y - y_0)\sin\theta}{v}, \tag{2}$$

where y_0 is the vertical position of the central element of the subarray on which the time-delay beamforming is performed and v is the material propagation velocity in the vicinity of each subarray, which is assumed to be homogeneous.

The DBF procedure involves first forming a 3D matrix of amplitude versus t, θ_r, θ_s, by varying the angles θ_r and θ_s between -90° and $+90^\circ$ with a step of 5°. The maximum amplitude in this 3D matrix is thus identified and the sampling in t, θ_r, θ_s is progressively refined in this region of interest up to 0.5° to give an optimized combination of t, θ_r, and θ_s. Thus the recorded signals for propagation between the central transducers of each of the source and receiver subarrays [see Fig. 3(a) for the case of facing transducers] are substituted by the beam-formed signals corresponding to the optimal $(\theta_r,\,\theta_s)$ pair. An example of the resulting signals is shown in Fig. 3(b). To facilitate the identification of the arrivals in this representation, the amplitude of the signal $p_{\mathrm{DBF}}(t,\,\theta_r,\,\theta_s)$ is replaced by its envelope, calculated through the Hilbert transform. Figure 3(c) shows an example of a slice through the resultant 3D matrix for a fixed time.

If the study material is reasonably homogeneous, only one high amplitude spot is present in the $(\theta_r,\,\theta_s,\,t)$ plot and the corresponding θ_s and θ_r will be close to the straight path θ_0 [$\theta_0 = 0$ in the example presented in Figs. 3(c) and 3(d)]. In the case of strong heterogeneities in the velocity field or in the vicinities of the boundaries (where reflections cannot be neglected), the transmitted wave field cannot be well described by single ray-paths between each source-receiver pair and so it can often be difficult to interpret the raw data because of interactions of multiple arrivals along different paths; these interactions can be destructive such that, apparently, no signal arrives. The use of DBF in these cases is essential because it allows separation of different arrivals: Different paths will have distinct take-off angles and/or distinct arrival angles, so the amplitude peaks will be separated in angle-time space (see Fig. 4). Each local maxima in $(\theta_r,\,\theta_s,\,t)$ space identifies a different arrival, which is characterized by the amplitude field $p_{r0,s0}(t,\,\theta_r,\,\theta_s)$ for the corresponding angles.

The described DBF analysis has been applied to the data presented in Fig. 2(b), acquired *post-mortem* on the natural rock sample. In this example the highly localized deformation between the notches leads to multiple arrivals and two wave fronts can be separated by the DBF procedure. Based on these separated signals it is possible to identify an arrival time for each propagation path [see Figs. 2(c), 2(d), and 4]. In particular Figs. 4(a) and 4(b) show an example of signals, traversing the deformed region of the sample, transmitted/received by the central transducer of the subarrays and obtained from DBF analysis, respectively. In this case, it is clear how from the raw signal (i.e., using standard approaches) it is not possible to extract the arrival time while DBF permits to separate these signals and then to retrieve the desired information. Moreover, later arrivals that can be due to reflections or presence of secondary waves (generated from P- to S-waves conversion) are naturally removed.

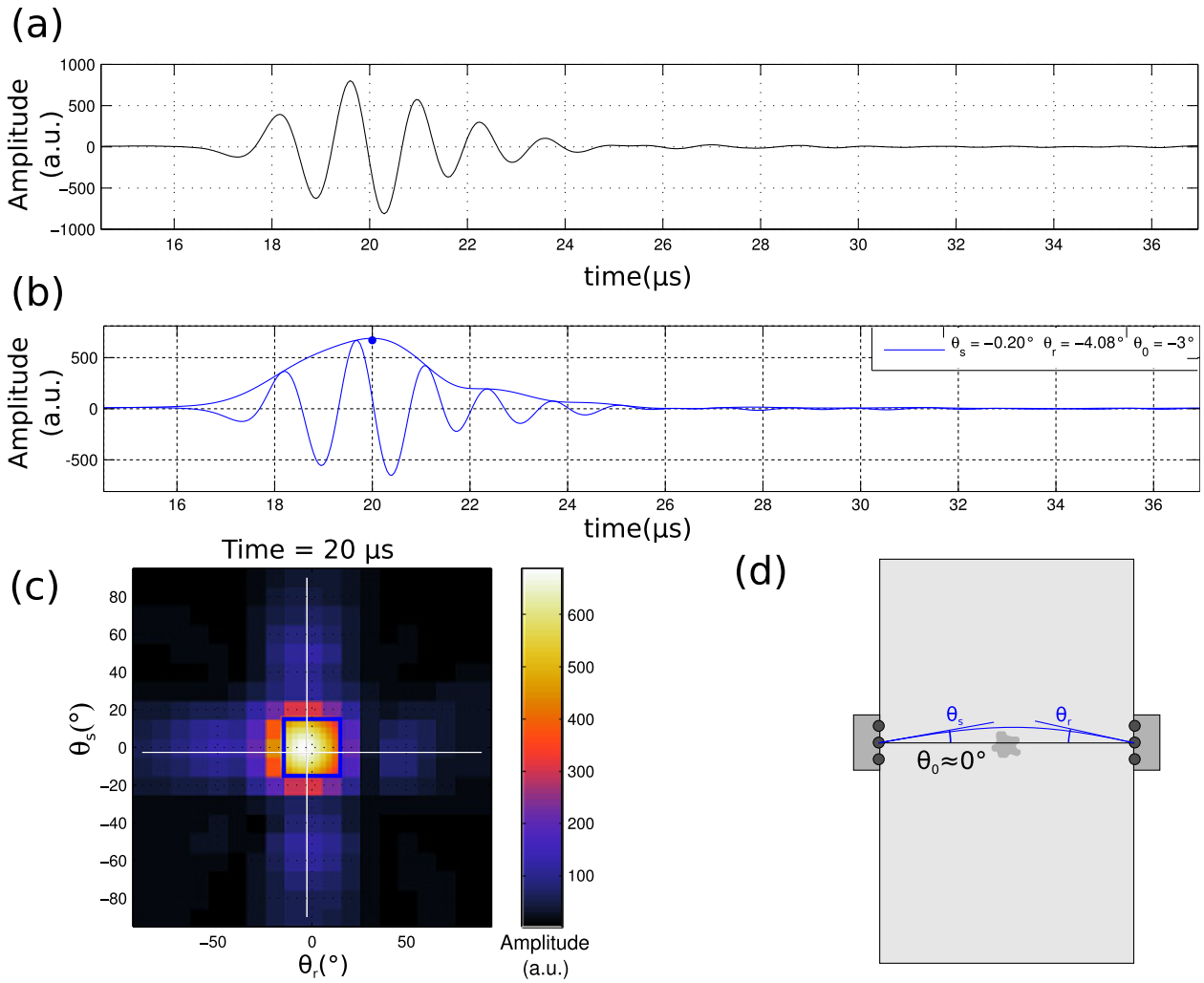

FIG. 3. (Color online) Signal transmitted by the central transducer through an intact sample of natural rock and received by the central transducer of two facing subarrays (a); the signal obtained from DBF and its envelope (b); a slice through the 3D matrix, resulting from DBF in which one amplitude peak can be identified (c); schematic of a ray-path in the presence of a small heterogeneity (d).

In addition to allowing signal separation and identification of travel times, two additional benefits of the DBF are information on take-off and arrival angles, which are otherwise unknown, and improvement of the signal-to-noise ratio. The take-off and arrival angle information might be used to better describe propagation paths, as presented later, and the signal-to-noise improvement can be on the order of $10\log_{10}(N_rN_s)$ dB (as shown by Iturbe[21]).

The described DBF approach can also be used for the identification of arrivals in a time lapse test, e.g., during loading. In this case, the DBF is applied to the first acquisition data set, for an angle range $[-90°{:}90°]$, and the maximum amplitude closest to the couple of angles corresponding to the direct path (θ_0, θ_0) is selected, assuming only a small deviation from homogeneity at the start. The DBF for any subsequent data set, acquired at a later step of loading, is only assessed in the vicinity of the couple of angles (θ_s, θ_r) selected at the previous step. This automatic procedure currently allows the selection of only one signal per source/receiver subarray couple, but it could be extended in the future to consider more than one arrival in the inversion process, corresponding to the different amplitude peaks visible in the DBF data.

A drawback of the DBF procedure is deviation from the assumption of point sources and receivers, which could potentially lead to reduced resolution. As such, the optimal subarray size results from a balance between resolution and robustness.[22–24] Large subarrays provide enhanced angular resolution. However, when there are strong heterogeneities close to the transducer arrays, as is often the case for geomaterials (where localized deformations may spread across the entire sample), beamforming performs better with shorter subarrays. In fact, when the subarray is positioned across a heterogeneity, the DBF result can be strongly affected. Moreover, the benefits due to an increasing array size are to be weighed against an increasing computation time and a loss of spatial resolution in terms of arrival time and take-off/arrival angle maps. Despite attempts to find an objective criterion to define the best subarray size, this remains a case-dependent problem and a parametric study is required (as shown by Turkaya[25]). In the current example, the DBF array sizes were chosen to be 7, for the case of the 64-transducer

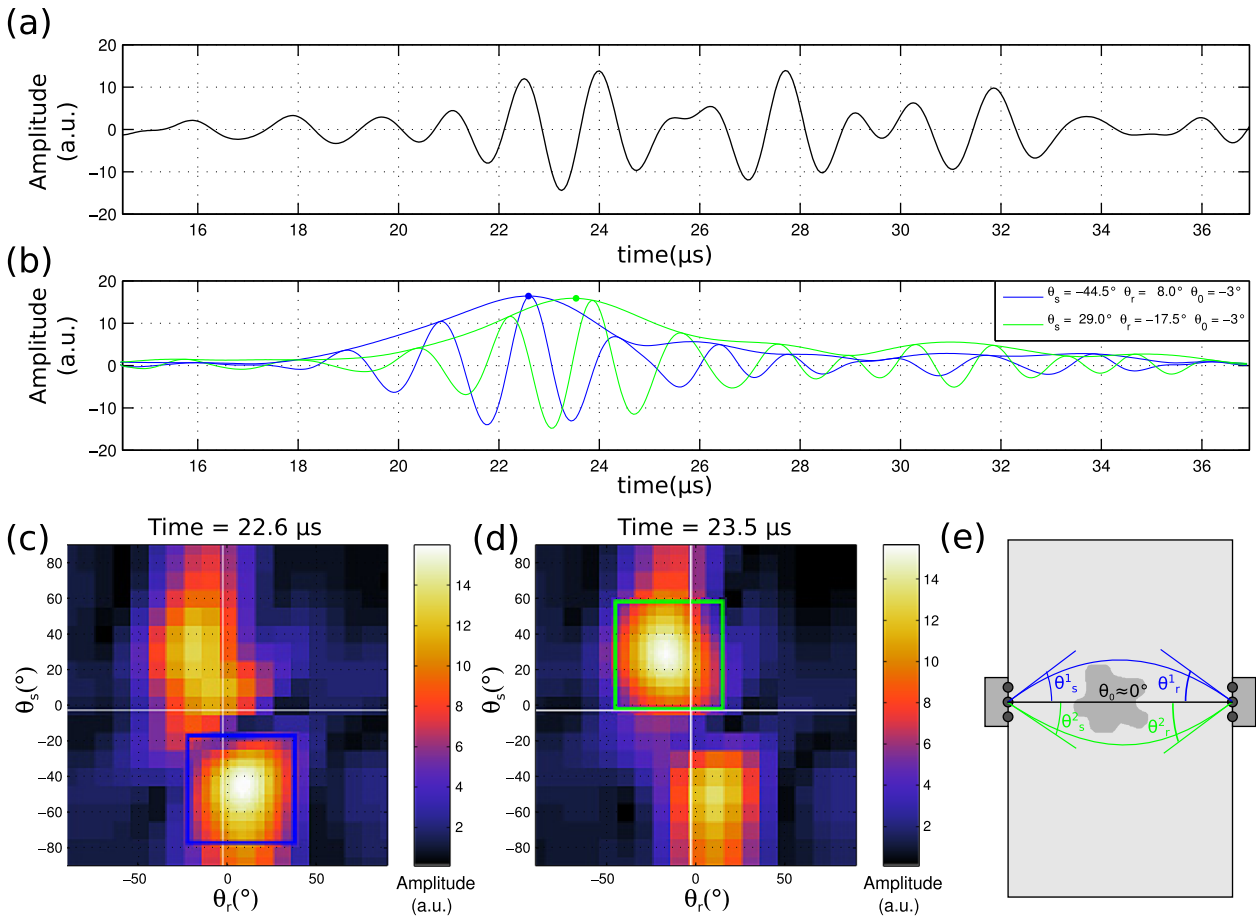

FIG. 4. (Color online) Signal transmitted/received through a deformed sample of natural rock by the central transducer of two facing subarrays (a); the two signals obtained from DBF, relative to two pairs of angles (b); slices through the 3D matrix, resulting from DBF, for two different times, in which two amplitude peaks can be identified [(c) and (d)]; schematic of two ray-paths corresponding to a wave having a distorted wave front due to a heterogeneity (e).

arrays, and 5, for the case of the 32-transducer arrays, on both the source and receiver sides.

B. Data extraction

The travel time between a source-receiver subarray pair is defined by comparing the DBF signal corresponding to the optimal angles (θ_s, θ_r) to a reference wavelet, with the same spectrum, propagating into a homogeneous medium, as described below.

A travel-time difference, Δt, between each of the DBF beams from the acquired data and a reference wavelet can be calculated from the phase shift of the inter-spectrum at the central frequency ω,

$$\Delta t = \frac{1}{\omega} \angle \left(\frac{X_i(\omega)}{X_0(\omega)} \right), \tag{3}$$

where $X_i(\omega)$ is the Fourier transform of the DBF signal $x_i(t)$, X_0 is the Fourier transform of the reference signal $x_0(t)$, and the symbol $\angle$ indicates the phase.

Performing the process described above for all source-receiver subarray pairs provides the full time-delay matrix for one acquisition [see Fig. 5(a)]. In this matrix, the rows represent the central sources and the columns the central receivers of subarrays so that the diagonal elements correspond to horizontal paths, while top-left and bottom-right corners correspond to the maximum inclined paths. This representation permits to assess the extracted data that are subsequently used as input to the travel-time inversion, as all the data can be visualized simultaneously in a structured way, making it possible to recognize any inconsistency between neighboring transducers and identify potential artifacts.

A matrix of take-off and arrival angles from the DBF procedure can also be retrieved. This information can be used to trace cubic rays for all source-receiver subarray pairs, using the positions of the two subarray central transducers and the take-off and arrival angles to define the corresponding third degree polynomial. Figure 5(b) shows a selection of cubic rays traced for the *post-mortem* measurements. The representation of cubic ray-paths gives preliminary information regarding the position and intensity of the heterogeneities. In particular, a less dense area is visible in the bottom left part of the sample, indicating a lower velocity patch. These ray-paths also provide a better initial estimate of the propagation than the common straight-ray assumption, as described in Sec. III C.

It can also be noted that the inter-spectrum phase shift analysis also provides an efficient, consistent means to determine travel-time differences between successive shots during a time-lapse acquisition, e.g., during loading. Each DBF

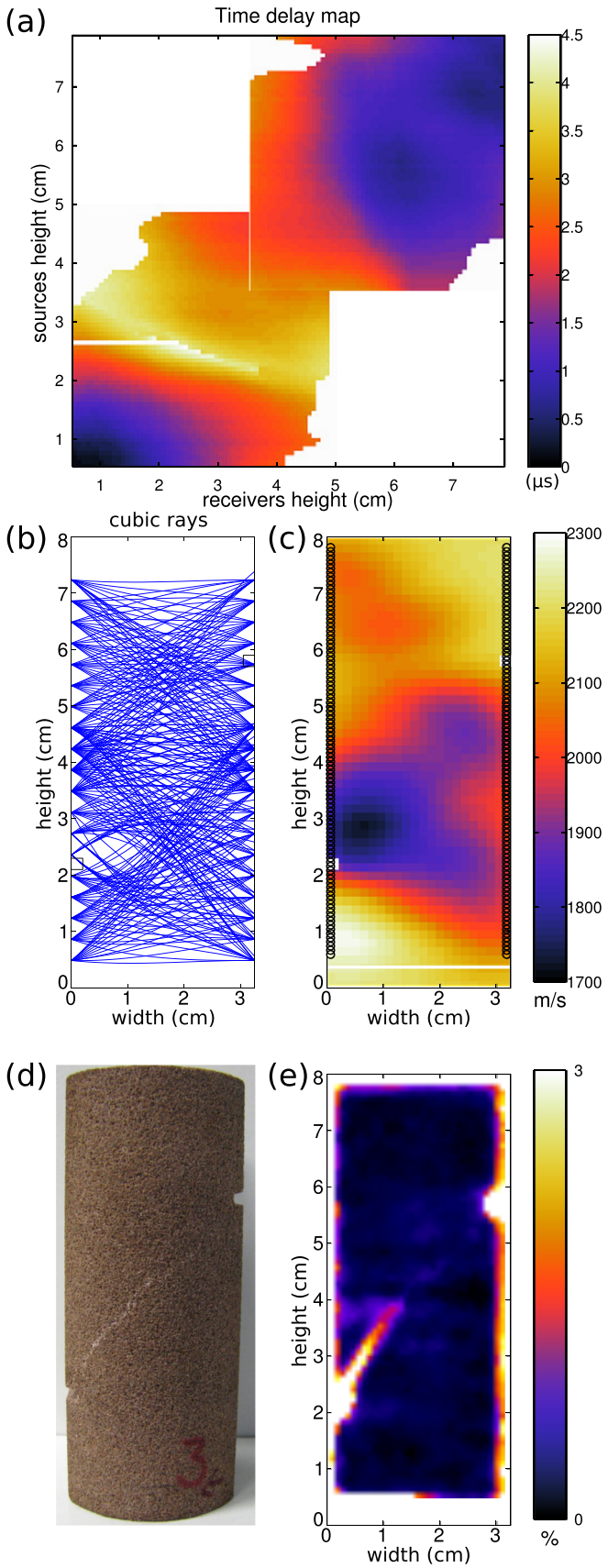

FIG. 5. (Color online) Time delay map, for the natural rock sample, calculated with respect to a homogeneous velocity field of 2200 m/s (a), a selection of cubic rays traced using the DBF results (b) and corresponding model based ultrasonic tomography (c); picture of the deformed sample (d); median, over the width of the sample, of the maximal shear deformation from the 3D-volumetric DIC analysis (e).

signal of a source-receiver subarray pair can be compared to the signal of the same pair at the previous shot to get the incremental travel-time change during the time-lapse sequence.

C. Inversion

Once the travel-time difference data have been acquired for all the source-receiver subarray pairs with travel paths crossing the area of interest an inversion procedure can be performed to derive a map of velocity changes in a sample. This is referred to as tomographic inversion. Such an inversion requires a forward model for wave propagation. In the case of ray theory the forward problem can be expressed by the relation

$$\delta t = \int_{\Gamma} -\frac{\delta v}{v^2} ds, \tag{4}$$

where δt is the travel-time difference between a source-receiver subarray pair, ds is the curvilinear distance along the ray path Γ, and δv is the scalar velocity perturbation associated to the change of the p-wave velocity v at every point in the sample.

The inversion of Eq. (4) will be referred to as *differential tomography* herein. Differential tomography can be "data-based," when the Δt's are evaluated using two sets of ultrasonic recordings acquired at two different times (for instance after a step of loading), or "model-based," when the Δt's are related to an initial-guess velocity field (often homogeneous). Note that the latter is the "standard" tomographic approach. With data-based inversion, one data set will be referred to as "reference" and the other as "current." Furthermore, in a time-lapse, data-based inversion, the difference of arrival times $\Delta\mathbf{t}$, and thus the velocity evolution, can be calculated referring always to the same acquisition file, for instance, the first one in a time-lapse sequence, or step-by-step (in the step-by-step approach, the current file will become the reference one at the subsequent step). Finally, to recover the absolute values of velocities, it is necessary to make a guess of the velocity field corresponding to the reference file.

To solve the inverse problem, the observed sample is spatially discretized into cells, in each of which the velocity is considered to be constant. In this manner Eq. (4) can be rewritten in matrix form as

$$\Delta\mathbf{t} = \mathcal{M} \cdot \Delta\mathbf{v}, \tag{5}$$

where $\Delta\mathbf{t}$ is the data vector of dimension $[1 \times m]$ with m the number of data (i.e., the number of subarray pairs), $\Delta\mathbf{v}$ is a vector of dimension $[1 \times n]$, with n the number of cells in which the model has been discretized, and $\mathcal{M}$ is a matrix of dimension $[m \times n]$ with $M_{ij} = -l_{ij}/v_j^2$ where l_{ij} is the length of the ith ray-path through the jth cell.

The simplest way to trace ray-paths, and then to construct the $\mathcal{M}$ matrix, is to consider straight lines. In this work an alternative propagation model, using cubic rays, is proposed.

The concept of cubic rays is not a usual one and has been identified as a means to enrich the linear inversion by using the additional information gained from the use of the DBF in the data processing. This approach depends on the velocity field only indirectly and remains a linear inversion problem (i.e., the $\mathcal{M}$ matrix construction is part of the data extraction process and it is not updated during the inversion), but, unlike straight rays, the ray-paths take into account the inhomogeneity of the velocity field. An example of the influence of the cubic rays in the inversion is given in Sec. IV. A wider analysis, including comparisons with curved rays obtained using Eikonal approximation, can be found in Tudisco[26] and Boué *et al.*[27]

It should be underlined that the output of DBF is the time delay across the local subarray, which can be transformed into angles only through a hypothesis on the local velocity. In cases where significant velocity variations occur at the boundaries of the sample (e.g., due to localized damage in the current example), the initial hypothesis of homogeneous velocity can lead to significant errors on take-off and arrival angle evaluation. A possible approach to take into account this phenomenon and then improve the cubic rays tracing, is to re-perform the DBF using, for each subarray, the local velocity from the inverted velocity field. This iterative approach was not applied in the present work and will be a topic for future work.

The number of travel time data is not necessarily equal to the number of unknowns (i.e., the number of cells). It follows that the matrix $\mathcal{M}$ is not necessarily square, so its inverse $\mathcal{M}^{-1}$ does not exist. Equation (5) can thus not be solved directly and a method to find a pseudoinverse must be used. In this work the Maximum *a posteriori* method[21] has been adopted. This method is based on Bayes' theorem, which allows the introduction of *a priori* information on the data misfit and medium parameters in the inversion. The *a priori* model is $\Delta\mathbf{v}_0 = 0$, which means that no spatial heterogeneity is initially assumed. The data-misfit *a priori* is taken to be statistically Gaussian and centered so that, considering the observables to be independent, the data covariance matrix C_d is diagonal. The model covariance matrix C_m is set in such a way that the inverted velocity values are spatially correlated with correlation lengths λ_x and λ_y along the x and y axis, respectively. Under these assumptions the estimated velocity field can be calculated as

$$\widetilde{\Delta\mathbf{v}} = \mathcal{C}_m\mathcal{M}^T(\mathcal{M}C_m\mathcal{M}^T + \varepsilon\mathcal{C}_d)^{-1}\cdot\Delta\mathbf{t}. \quad (6)$$

The parameters that control the inversion are ε, which weights the model-versus-data *a priori*, and the characteristic correlation lengths λ_x and λ_y, which limit the variability of neighbor cell values. The higher ε, the more the resultant velocity field is influenced by prior information. This can thus be considered as a damping parameter that controls how fast the model can reach a solution. The correlation lengths provide a spatial smoothing and their values vary from zero to twice the wavelength depending on several factors including the physical model used. In this work, the choice of λ_x and λ_y was based on a parametric study made with synthetic and real data.

IV. APPLICATIONS AND VALIDATION

The procedure described above has been applied to the data obtained from the natural rock sample *post-mortem* to provide a demonstration of the applicability of the technique to investigate localization phenomena in laboratory samples.

Figure 5(a) presents the complete set of travel time data for the natural rock sample (positions 1 and 2) as a delay map, calculated with respect to a homogeneous velocity field of 2200 m/s, which is the mean propagation velocity in the intact rock; this velocity is also used as the background velocity in the inversion. Inversion of these data using model-based tomography provides the velocity field shown in Fig. 5(c). The first observation from the inverted velocity field is strong low velocity heterogeneity close to the bottom notch. Furthermore, three bands of reduced velocity can be identified, one connecting the two notches and two others going diagonally up and down from the top and bottom notch, respectively. The band between the notches and the one going downwards from the bottom notch are well formed while the band heading upwards from the top notch is less well defined. This result is in agreement with the expected deformation structure, i.e., a localized band of deformation that likely involves grain and grain-contact breakage and thus reduced velocities. The location of these bands is in agreement with observations from other full-field measurement techniques, i.e., x-ray tomography and 3D-DIC.[19] In particular the central low velocity band is clearly visible on the surface of sample, see Fig. 5(d), and in the example of 3D-DIC analysis, shown in Fig. 5(e), which represents the median over the width of the sample of the maximal shear strain. The low velocity band on the bottom of the sample is only partially visible in this image while the band on the top is invisible. This indicates that the occurring micro-mechanisms, responsible for the decrease of the wave propagation velocity, are not strong enough to induce a deformation that can be detected by the 3D-DIC analysis. The strong velocity heterogeneities around the notches in fact cause the wave fronts to split and, therefore, at least two wave fronts are registered (e.g., Fig. 2). However, despite the DBF procedure permits the identification of multiple arrivals for each source-receiver couple [Figs. 2(c), 2(d), and 4], only one of them has been used in the current inversion. Considering multiple paths may be helpful to increase spatial resolution in future work. It is noted that the significant heterogeneity in the velocity field, especially around the notches, will also have an effect on the spatial resolution through the variable ray-coverage as indicated in Fig. 5(b).

The data analysis and inversion procedure has also been applied to data acquired during loading for a sample of rock into which an inclined layer of cemented sand was introduced. This application had two objectives: First, to provide a validation, with a sample of well-defined geometry, of the ability of the method to resolve velocity heterogeneities, as those observed in the natural rock example presented above; second, to provide a test case to extend the method to time-lapse analysis of *in situ* measurements during mechanical loading of a sample.

The schematic of the controlled-geometry sample and the wave acquisition system integrated into the loading

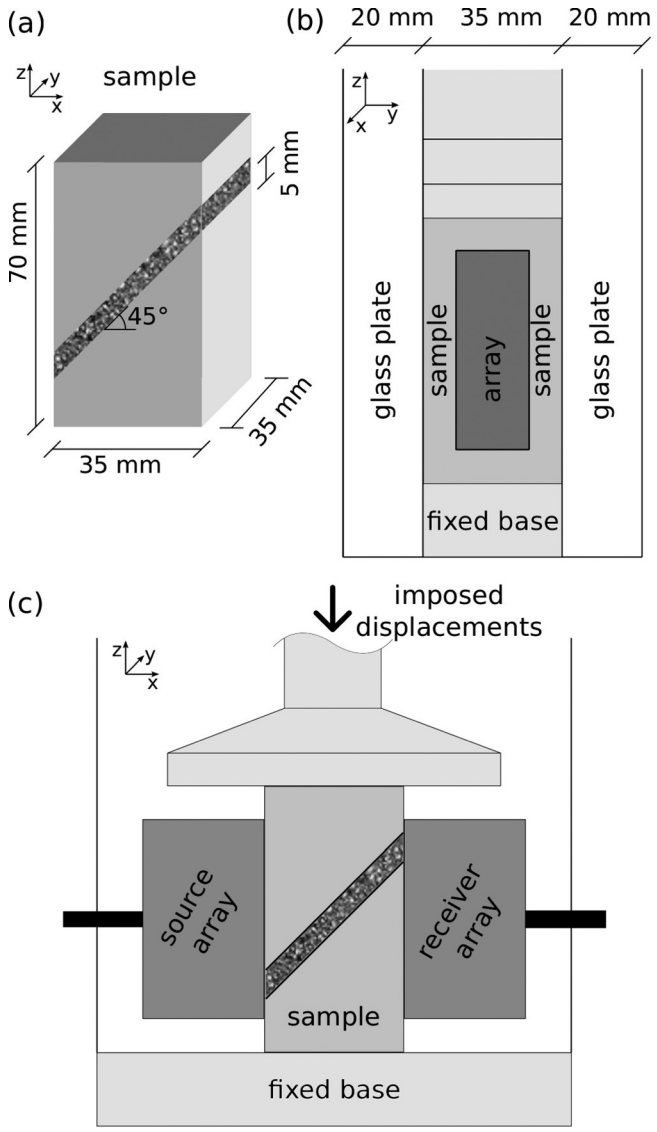

FIG. 6. Schematic of the constructed sample (a) and of the wave acquisition system integrated into the loading device [(b) and (c)].

device are presented in Fig. 6. To study the evolution of the propagation velocity field in the sample during mechanical loading by time-lapse tomography, it is important to assure the repeatability of the measurements, in particular regarding the position of the transducers. Therefore the arrays were held in fixed positions and only the central part of the sample was imaged. The controlled-geometry sample was prismatic and was loaded in plain strain conditions (guaranteed by two thick glass plates) to reduce the problem to 2D.

The first aim of this example is to assess the resolution of the ultrasonic tomography in a simplified situation in which the geometry of the problem is known. A central vertical slice of an x-ray tomography image of the sample is presented in Fig. 7(a); this shows the well-defined structure of the artificial layer. Based on data acquisition before any loading of the sample, DBF analysis was performed and cubic rays traced; the ratio between cubic and straight ray-density distribution is shown in Fig. 7(b). Subsequently model-based tomographies were carried out using cubic and straight rays [Figs. 7(c) and 7(d), respectively]. Figure 7(e)

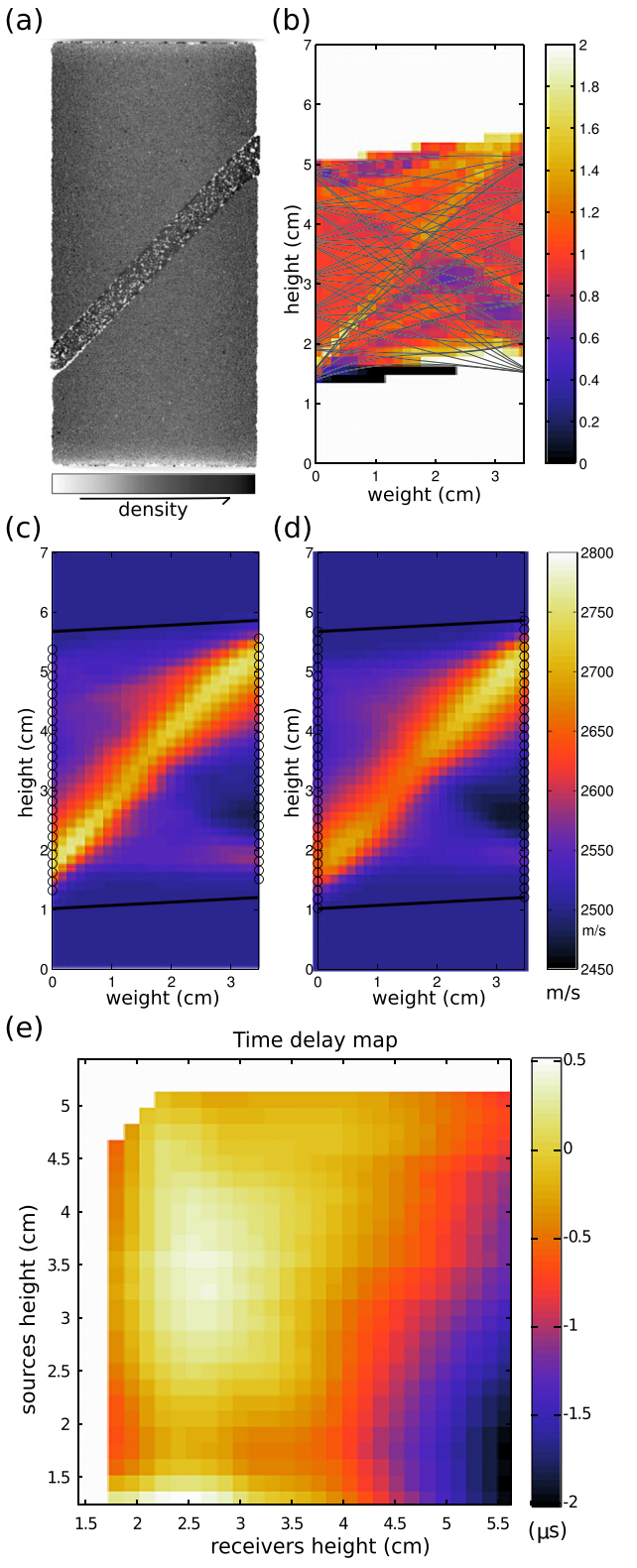

FIG. 7. (Color online) X-ray tomography central slice of the constructed sample (a); distribution of the cubic/straight ray density ratio (b); model based ultrasonic tomographies obtained with cubic rays (c) and straight rays (d); corresponding time delay map calculated with respect to a homogeneous velocity field of 2500 m/s (e). The circles indicate the positions of the transducers and the black lines delimit the area of the sample affected by the inversion.

shows the time delay map, calculated with respect to a homogeneous velocity field of 2500 m/s or the background velocity used in the inversion. The results of these

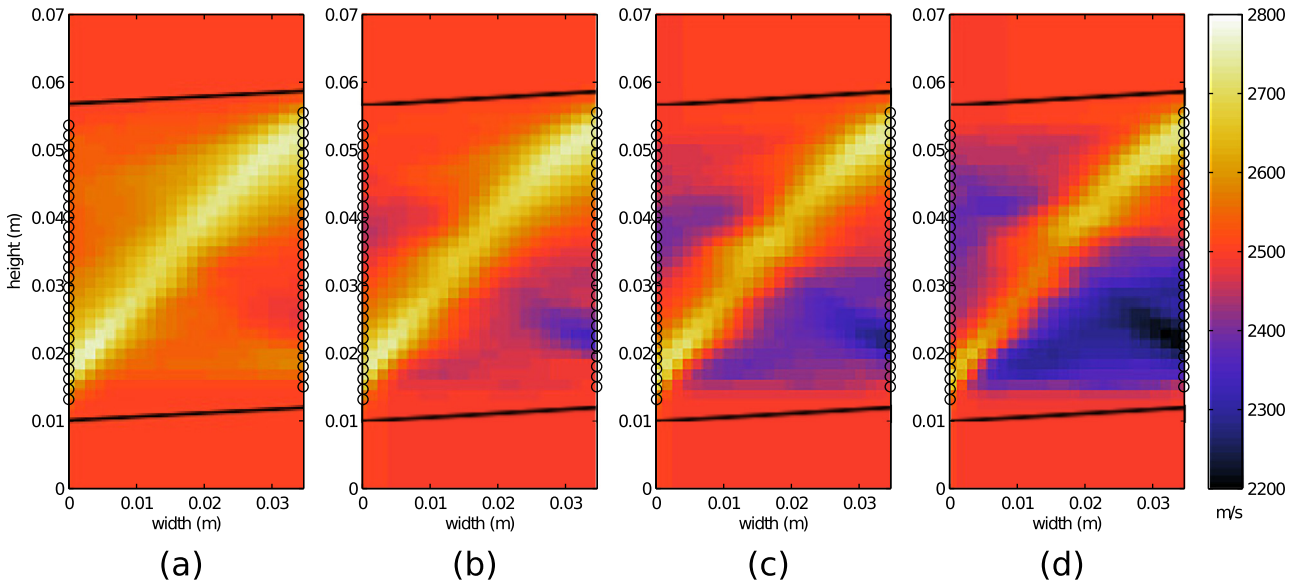

FIG. 8. (Color online) Velocity field evolution calculated through data based ultrasonic tomographies. Images correspond to the initial stage (a) and to axial strain of 0.75% (b), 0.9% (c), and 1.05% (d).The circles indicate the positions of the transducers and the black lines delimit the area of the sample affected by the inversion.

model-based tomographies show, in both cases, a well defined inclined layer of high velocity, which is consistent, in terms of both the inclination and band thickness, with the actual structure [Fig. 7(a)]. The velocity field obtained using cubic rays, however, exhibits a sharper and more uniform high velocity band. This result confirms that the spatial resolution of the ultrasonic tomography is about 5 mm, which corresponds to twice the wavelength of the examined signals. The higher velocity inside the layer implies that, as the mean density (indicated by x-ray tomography) is comparable in the two materials, the cemented sand is stiffer than the surrounding rock. This could indicate that the grains in the layer of artificially cemented sand are more bound and that the natural cementation is weaker than the artificial one.

After the above verification of the tomography approach for model-based inversion, time-lapse data acquired during mechanical loading of the layered-geometry sample were analyzed by data-based inversion. The objective in this application was to investigate the time-lapse tomography as a way to monitor damage evolution processes during laboratory experiments for future investigations of rock deformation process. Data-based tomography was carried out following the step procedure with a step increment of 10 files (data were acquired every 45 s). Figure 8 shows the velocity fields corresponding to the initial stage and three subsequent stages of loading. While the sample at the end of the test did not show any visually detectable deformation, the presented images reveal that, in a first phase, the velocity perturbations occur mainly outside the layer and that the velocity in these regions increases progressively. The velocity changes outside of the band are mostly negative, i.e., decreasing velocity, suggesting that the rock damages during the loading. A stronger reduction of velocity is registered on the right-side of the sample. This low velocity area, however, is also visible in the initial velocity image and, indirectly, in the cubic ray-density distribution, which suggests that the mechanical properties in that zone are different from the surrounding material from the beginning. It is, therefore, reasonable to suggest that the damage caused by the loading could be different in this zone, and more specifically that the zone is weaker (perhaps due to lower cementation, which would give lower velocities) and thus experiences greater damage. Furthermore, there seems to be a correspondence in the time-delay matrix. In a later stage, a decrease of velocity is registered inside and outside the layer. This indicates that damage occurs in both the artificially cemented sand and the natural rock, but the latter is weaker and damages at smaller macroscopic strain; this is in agreement with the model-based tomography results indicating stronger cementation inside the layer than outside. Furthermore, when the velocity inside the layer reduces, the contrast between the natural rock and the cemented sand is reduced resulting in an apparent decrease of the layer thickness, especially at the bottom of the sample.

V. CONCLUSIONS

Elastic wave measurements are often used to study the behavior of geomaterials both at the laboratory scale and at the field scale. The novelty of this work is the implementation of travel-time inversion techniques, of the type used in oceanography and geophysics, to laboratory geomechanics. In particular, array processing methods have been applied to a geometry similar to seismic cross-hole tomography, but at an entirely different scale. Moreover, ultrasonic tomography has been used to monitor time-lapse damage evolution.

In terms of the data analysis prior to the velocity inversion, a new approach has been suggested based on double beamforming. The implementation of double beamforming

in the particular case of a laboratory test on geomaterials provides improved quality data and thus permits extraction of accurate travel-time information. Furthermore, using this approach allows separation of arrivals from different propagation paths, which can provide data in complex areas where interfering arrivals make travel time picking impossible, with standard approaches, increasing the available data for the inversion. Moreover, the information on take-off/arrival angles can be used to trace cubic rays, which take indirectly into account the inhomogeneity of the velocity field. At present, when multiple arrivals are separated, only the one closest to the straight ray path is considered in the inversion. The use of the other extracted signals could be implemented in the inversion exploiting the cubic ray's tracing.

The proposed ultrasonic tomography procedure has been used to investigate localized deformation in a sample of natural rock that has undergone triaxial compression. In this case, the sample had notches on both sides to encourage localized deformation, in the form of a shear band, to occur in the middle of the sample. The ultrasonic tomography revealed the presence of three localized bands of low velocity, one connecting the notches and the others extending from the notches to the top and bottom sample's boundaries. The localized deformation had been imaged using x-ray tomography and by 3D-DIC analysis from which only the band connecting the two notches was partially visible. The ultrasonic tomography can therefore reveal structures undetectable by other techniques as well as indirect information about micro-mechanism such as grain and cement breakage.

To determine the spatial and temporal resolution of the ultrasonic tomography in a simplified situation, tests were carried out on a sample consisting of a layer of cemented sand between two blocks of natural rock. The contrast between the material properties of the cemented sand and the natural rock results in two distinct propagation velocities inside and outside the layer making the initial geometry of the velocity field known *a priori*. The comparison between a model-based ultrasonic tomography and an x-ray tomography of the intact sample showed that the 5 mm thick layer of cemented sand could be well resolved and thus the resolution of the ultrasonic inversion respects the expectation (about twice the wavelength of the transmitted signals). Subsequent analysis of data acquired during loading of the sample allowed testing of the time-lapse ultrasonic tomography approach for damage field characterization. The model-based and the time-lapse ultrasonic tomography analysis revealed that the layer is stiffer than the rock and that the latter damages before during the loading. This is probably due to a weaker cementation of the grains in the natural rock.

The results presented in this paper demonstrate that ultrasonic tomography can provide clear information on damage localization and evolution in laboratory specimens, with a good resolution. Combining such measurements with other experimental geomechanics approaches (e.g., x-ray tomography and DIC) will allow enhanced investigation of the micro-mechanisms of failure, such as cement breakage and grain de-bonding, in cemented granular materials. Another perspective is to implement a fully automated procedure for the data processing; such a procedure, which would currently take about 1 h for 32×32 signals, would enable more real-time monitoring in quasi-static deformation experiments.

[1]G. Viggiani and S. Hall, "Full-field measurements, a new tool for laboratory experimental geomechanics," in *Proceedings of the 4th Symposium on Deformation Characteristics of Geomaterials* (IOS Press, Amsterdam, 2008), Vol. 1, pp. 3–26.

[2]G. Viggiani, S. Hall, and E. Romero, eds., *ALERT Doctoral school 2012—Advanced Experimental Techniques in Geomechanics* (The Alliance of Laboratories in Europe for Research and Technology, Grenoble, 2012), pp. 3–67.

[3]H. Iyer and K. Hirahara, *Seismic Tomography: Theory and Practice* (Chapman & Hall, London, 1993), pp. 1–875.

[4]J. Berryman, "Lecture notes on nonlinear inversion and tomography: 1. Borehole seismic tomography," Technical Report, Lawrence Berkeley National Laboratory, CA (1991), pp. 1–142.

[5]D. Vasco and E. Majer, "Wavepath traveltime tomography," Geophys. J. Int. **115**, 1055–1069 (1993).

[6]M. Van Schaack, "Calculating Fresnel zones for crosswell tomography," Stanford Tomography Project, Stanford (1994), pp. C-1–C-15.

[7]R. Brossier, S. Operto, and J. Virieux, "Seismic imaging of complex onshore structures by 2d elastic frequency-domain full-waveform inversion," Geophys. **74**, WCC105–WCC118 (2009).

[8]J. Virieux and S. Operto, "An overview of full-waveform inversion in exploration geophysics," Geophysics **74**, WCC1–WCC26 (2009).

[9]C. Chapman and R. Pratt, "Traveltime tomography in anisotropic media—I. Theory," Geophys. J. Int. **109**, 1–19 (1992).

[10]R. Pratt and C. Chapman, "Traveltime tomography in anisotropic media—II. Application," Geophys. J. Int. **109**, 20–37 (1992).

[11]S. A. Hall, "When geophysics met geomechanics: Imaging of geomechanical properties and processes using elastic waves," in *Mechanics of Natural Solids* (Springer-Verlag, Berlin, 2009), pp. 147–175.

[12]W. Debski and R. Young, "Enhanced velocity tomography: Practical method of combining velocity and attenuation parameters," Geophys. Res. Lett. **26**, 3253–3256, doi:10.1029/1998GL010368 (1999).

[13]T. Scott and Y. Abousleiman, "Acoustical imaging and mechanical properties of soft rock and marine sediments: Final technical report #15302," PoroMechanics Institute, The University of Oklahoma, Norman, OK (2004), pp. 1–136.

[14]J.-S. Lee, A. L. Fernandez, and J. C. Santamarina, "S-wave velocity tomography: Small-scale laboratory application," Geotech. Testing J. **28**, 1–9 (2005).

[15]R. Mitra and E. Westman, "Investigation of the stress imaging in rock samples using numerical modeling and laboratory tomography," in *12th International Conference on Computer Methods and Advances in Geomechanics*, Goa (2008), Vol. 2, pp. 1075–1082.

[16]E. Charalampidou, "Experimental study of localized deformation in porous sandstones," Ph.D. thesis, Heriot Watt University and Universite de Grenoble (2011).

[17]E.-M. Charalampidou, S. A. Hall, S. Stanchits, H. Lewis, and G. Viggiani, "Characterization of shear and compaction bands in a porous sandstone deformed under triaxial compression," Tectonophysics **503**, 8–17 (2011).

[18]P. Besuelle, J. Desrues, and S. Raynaud, "Experimental characterization of the localization phenomenon inside a Vosges sandstone in a triaxial cell," Int. J. Rock Mech. Mining Sci. **37**(8), 1223–1237 (2000).

[19]E. Tudisco, "Utrasonic and x-ray tomographies to study localized deformation in sandstone," Master's thesis, Université Joseph Fourier Grenoble INP (2009).

[20]P. Roux, B. D. Cornuelle, W. A. Kuperman, and W. S. Hodgkiss, "The structure of ray-like arrivals in a shallow-water waveguide," J. Acoust. Soc. Am. **124**, 3430–3439 (2008).

[21]I. Iturbe, P. Roux, B. Nicolas, J. Virieux, and J. Mars, "Shallow-water acoustic tomography performed from a double-beamforming algorithm: Simulation results," IEEE J. Ocean. Eng. **34**, 140–149 (2009).

[22]C. Marandet, P. Roux, B. Nicolas, and J. Mars, "Target detection and localization in shallow water: An experimental demonstration of the acoustic barrier problem at the laboratory scale," J. Acoust. Soc. Am. **129**, 85–97 (2011).
[23]F. Aulanier, B. Nicolas, P. Roux, and J. I. Mars, "Time-angle sensitivity kernels for sound-speed perturbations in a shallow ocean," J. Acoust. Soc. Am. **134**, 88–96 (2013).
[24]P. Roux and B. Nicolas, "Inverting for deterministic surface gravity wave using the sensitivity kernel approach," J. Acoust. Soc. Am. **135**(4), 1789–1799 (2014).
[25]S. Turkaya, "Improvements to ultrasonic data analysis for full field damage evolution mapping in soft rocks," Master's thesis, Université Joseph Fourier Grenoble INP (2012).
[26]E. Tudisco, "Development and application of time-lapse ultrasonic tomography for laboratory characterization of localized deformation in hard soils/soft rocks," Ph.D. thesis, Universite de Grenoble and Universita degli studi di Roma "Tor Vergata," 2013.
[27]P. Boué, P. Roux, M. Campillo, and B. Xavier, "Phase velocity tomography of surface waves using ambient noise cross correlation and array processing," J. Geophys. Res.: Solid Earth **119**, 519–529 (2014).